PROCEEDINGS OF THE EURO-C 1998 CONFERENCE ON COMPUTATIONAL MODELLING OF CONCRETE STRUCTURES/BADGASTEIN/AUSTRIA/31 MARCH - 3 APRIL 1998

Computational Modelling of Concrete Structures

Edited by

René de Borst
Faculty of Civil Engineering, Delft University of Technology, Netherlands

Nenad Bićanić
Department of Civil Engineering, University of Glasgow, UK

Herbert Mang & Günther Meschke
Institute for Strength of Materials, Technical University of Vienna, Austria

OFFPRINT

A.A.BALKEMA/ROTTERDAM/BROOKFIELD/1998

Computational Modelling of Concrete Structures, de Borst, Bićanić, Mang & Meschke (eds)
© 1998 Balkema, Rotterdam, ISBN 90 5410 946 7

Punching shear in reinforced concrete: Localized process

Ph. Menétrey
Emch + Berger AG, Bern, Switzerland
K.J. Willam
University of Colorado, Boulder, Colo., USA

ABSTRACT: A finite element model has been developed to reproduce shear failure in reinforced concrete structures that may be characterized as follows: (1) the reinforcing steel and concrete are coupled by the assumption of full bond in R/C components (a bilinear stress-strain law describes the uniaxial behavior of the reinforcements), (2) the triaxial strength criterion of concrete is expressed as a function of three stress invariants, (3) the non-associated plastic rate of deformation determines the volumetric flow direction of concrete by a dilatancy angle which coincides in direct tension with the direction of uniaxial tension, (4) crack induced strain-softening controls the reduction of the tensile strength by an isotropic decohesion process monitored by constant fracture energy (the ductility of concrete failure under different stress is accounted for by the number of fictitious cracks), and (5) degradation of concrete stiffness due to cracking is captured by an isotropic elastic damage model.

The numerical simulation of a circular R/C slab supported by a circular column demonstrates that the finite element model reproduces the punching failure mechanisms observed experimentally: the formation of a flexural tangential crack over the column is followed by radial cracks and finally forms an inclined punching shear crack inside the slab. Furthermore, the punching load is captured.

A closer look at the shear failure mechanisms reveals that: (1) localized shear failure is initiated by the coalescence of micro-cracks inside the slab, followed by an inclined crack propagation, (2) shear failure is caused by tensile concrete cracking along the inclined crack, and (3) analysis of the acoustic tensor reveals that the compression-shear stress at the slab-column intersection is modified during loading and approaches a state of pure shear stress responsible for tensile crack propagation at punching failure.

1 INTRODUCTION

Reinforced concrete slabs supported on columns fail by punching-shear when the column suddenly perforates the slab after forming a conical shear plug. A review of this failure phenomenon has been presented by Regan and Braestrup (1985).

The approach adopted here is based on finite element simulation of this localized failure mechanism using a triaxial concrete formulation. The plasticity formulation of concrete is a continuum description of failure which is regularized by the discrete idealization of reinforcing bars along element edges. The R/C finite element model captures strain localization and describes constant fracture energy dissipation as described further on.

The first attempt to apply fracture mechanics to punching failure was reported by De Borst and Nauta (1985). Later González -Vidosa et al. (1988) and Dyngeland et al. (1994) investigated the capabilities of various material models to simulate punching failure. However, the localized punching failure mechanism was never clearly captured. More recently, Menétrey et al. (1997) proposed a finite element model to simulate punching shear which reproduced the localized mode of punching failure. This model is detailed in the following.

2 NUMERICAL MODEL

2.1 *Preliminaries*

At the constitutive level, the behavior of concrete is described within the framework of the flow theory of plasticity (see e.g. Chen (1982)). The nonlinear response of reinforcing steel and concrete is treated separately assuming full bond conditions. The steel behavior is characterized by a bilinear stress-strain response which is the same in tension and compression.

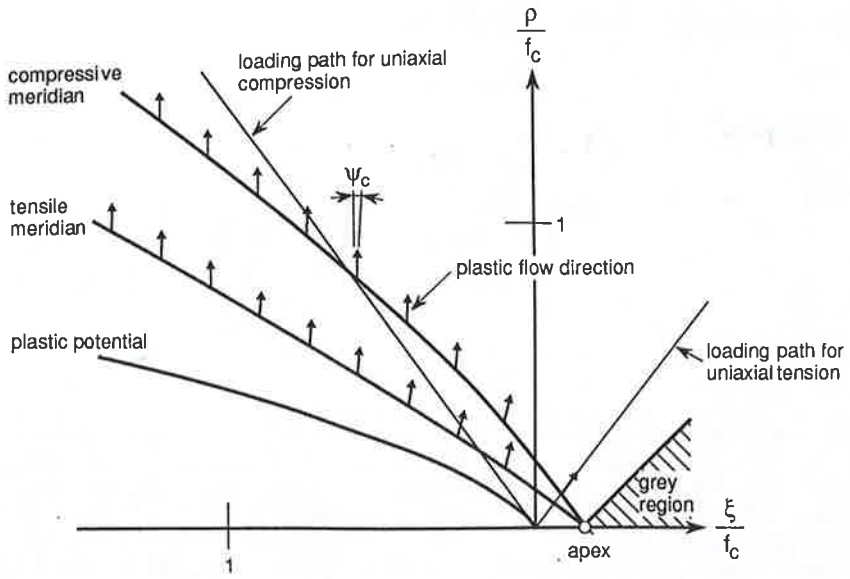

Figure 1: Concrete failure criterion, plastic potential, plastic flow direction, and grey region in the meridian plane

2.2 *Concrete failure criterion*

The triaxial criterion of concrete failure is a critical ingredient to describe punching failure as proposed by Moe (1961). The triaxial strength criterion developed by Menétrey and Willam (1995) is used in order to reproduce punching shear failure. The failure criterion is expressed in terms of the three invariants ξ, ρ, θ (which correspond to the hydrostatic and deviatoric invariants and the polar angle of the Haigh-Westergaard coordinates see e.g. Chen (1982)) of the stress tensor $\boldsymbol{\sigma}$ as:

$$f = \left[\sqrt{1.5}\frac{\rho}{f_c}\right]^2 + \phi\left[\frac{\rho}{\sqrt{6}f_c}r(\theta, e) + \frac{\xi}{\sqrt{3}f_c}\right] - c = 0, \tag{1}$$

where f_c denotes the uniaxial compressive strength. Initially, the cohesion parameter is set to $c = 1$, and the friction parameter is $\phi = 3\frac{f_c^2 - f_t^2}{f_c f_t}\frac{e}{e+1}$, whereby f_t is the uniaxial tensile strength. The elliptic function $r(\theta, e)$ is based on the 5-parameter model by Willam and Warnke (1974):

$$r(\theta, e) = \frac{4\left(1-e^2\right)\cos^2\theta + (2e-1)^2}{2\left(1-e^2\right)\cos\theta + (2e-1)\,D^{1/2}}, \tag{2}$$

with $D = 4\left(1-e^2\right)\cos^2\theta + 5e^2 - 4e$. The eccentricity parameter e describes the out-of-roundness of the deviatoric trace which is the limiting ratio of the tensile meridian over the compressive meridian:

$$e = \text{limit}(\text{as } \rho \text{ tends to } 0)\frac{\rho(\theta = 0)}{\rho(\theta = \pi/3)}. \tag{3}$$

Convexity and smoothness of the elliptic function requires that $0.5 < e \leq 1$. For $\phi > 0$ one singular apex is located at: $\xi = (c\sqrt{3}f_c)/\phi, \rho = 0$. The failure criterion is illustrated in the planes along the tensile (θ=0) and the compressive ($\theta = \pi/3$) meridians as well as the apex in Figure 1.

2.3 *Concrete flow rule*

The evolution of the plastic deformation is described with a flow rule derived from the plastic potential g such that:

$$\Delta\epsilon_p = \Delta\gamma\partial g/\partial\boldsymbol{\sigma}, \tag{4}$$

where $\Delta\gamma$ is the plastic multiplier and ∂ refers to the partial derivative. The plastic potential which was shown to appropriately simulate shear failure is expressed as:

$$g(\rho, \xi) = \rho^2 + B\rho + C\xi. \tag{5}$$

where parameters B and C define the axisymmetric shape.

The plastic flow direction is defined by the gradient of the plastic potential:

$$m_{ij} = \frac{\partial g}{\partial\sigma_{ij}} = \left(2 + B\frac{1}{\rho}\right)s_{ij} + \frac{C}{\sqrt{3}}\delta_{ij}. \tag{6}$$

The gradient is a function of the deviatoric stress $\boldsymbol{s}$

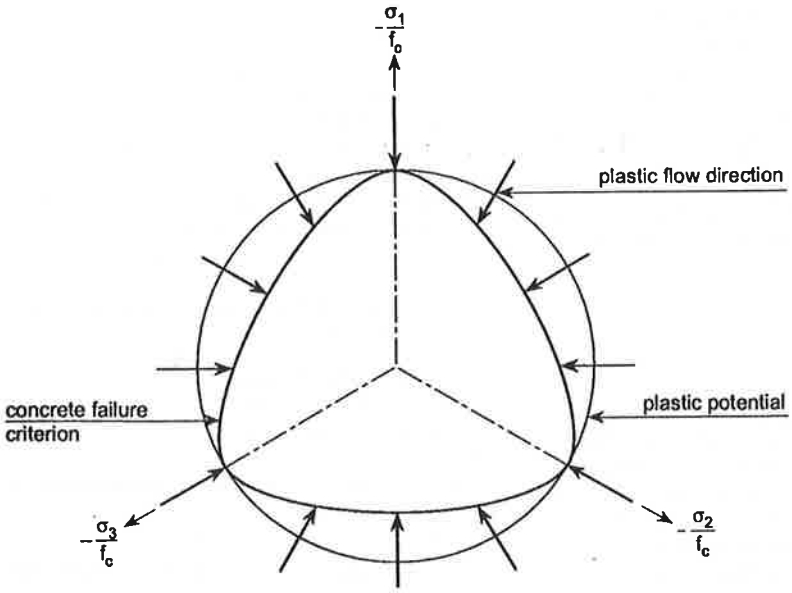

Figure 2: Plastic flow direction in the deviatoric plane

and a constant volumetric stress component. The parameters B and C are determined so that the dilatancy of plastic strains observed in triaxial experiments is reproduced. The following two conditions are satisfied:
(1) for the uniaxial tension test, the flow direction is fully aligned with the loading path of uniaxial tension (this condition reproduces the elastic unloading in the radial direction observed experimentally during uniaxial tension experiments on plain concrete),
(2) for the uniaxial compression test, the flow direction is described by the dilatancy angle ψ_c which introduces a new material parameter. These two conditions are graphically presented in Figure 1.

The first condition is satisfied if the slope of the loading path for uniaxial tension ($\xi/\rho = 1/\sqrt{2}$) equals the flow direction at the point of ultimate tensile strength ($\xi = f_t/\sqrt{3}, \rho = \sqrt{2/3}f_t, \theta = 0$). The slope of the flow direction is derived from Equation 6 by introducing the invariants: $\xi(\boldsymbol{m}) = C$ and $\rho(\boldsymbol{m}) = 2\rho + B$ so that the first condition gives

$$\frac{\xi}{\rho} = \frac{C}{2\rho + B} = \frac{1}{\sqrt{2}}. \tag{7}$$

This condition must be valid at the point of uniaxial tensile strength, which leads to

$$\frac{2}{\sqrt{3}} f_t + \frac{1}{\sqrt{2}} B = C. \tag{8}$$

The second condition states that at the point of ultimate compressive strength, ($\xi = -f_c/\sqrt{3}, \rho = \sqrt{2/3}f_c, \theta = \pi/3$), the flow direction is specified by the dilatancy angle ψ_c. This second condition is expressed as $\tan\psi_c = \xi/\rho$. Introducing the invariants of the flow rule leads to

$$\frac{2\sqrt{2}}{\sqrt{3}} \tan\psi_c f_c + \tan\psi_c B = C. \tag{9}$$

Combining Equations 8 and 9 results in

$$B = \frac{2(\sqrt{2}\tan\psi_c f_c - f_t)}{\sqrt{3}(1/\sqrt{2} - \tan\psi_c)}, \tag{10}$$

$$C = \frac{1}{\sqrt{2}} B + \frac{2}{\sqrt{3}} f_t. \tag{11}$$

The parameter B must remain strictly positive which implies that:

$$\arctan\left(\frac{f_t}{\sqrt{2}f_c}\right) < \psi_c < \arctan\frac{1}{\sqrt{2}} \approx 35.3^0, \tag{12}$$

for $f_c/f_t = 10$ this condition reads: $4^0 < \psi_c < 35.3^0$.

The shape of the plastic potential is circular in the deviatoric plane, which corresponds to a non-associated flow rule except if $e = 1$. This assumption illustrated in Figure 2 simplifies the formulation and facilitates the stress computation. It is neither in contradiction nor does it reproduce experimental results, as very few are available for validation.

The apex of the failure criterion results in a grey region in the stress space where the stress return algorithm is not defined. This grey region is illustrated in Figure 1. It is delimited by the condition

$$\xi \leq \rho \frac{C}{B} + \frac{c\sqrt{3} f_c}{\phi}. \tag{13}$$

If the trial overstress state is located in the grey region, it is returned to the apex of the failure criterion.

2.4 *Concrete cracking*

Concrete cracking is described by a smeared crack model using strain-softening which enforces a gradual decrease in tensile strength with increasing tensile deformation. The fictitious crack model developed by Hillerborg et al. (1976) is considered in which the tensile stress σ_t is directly controlled by crack opening w. The amount of energy per unit surface area absorbed in opening a crack from zero to the crack rupture opening displacement w_r is

$$G_f = \int_0^{w_r} \sigma_t dw, \tag{14}$$

defines the fracture energy which is dissipated during the tensile decohesion process and which constitutes a basic fracture property.

The gradual decrease in tensile strength with tensile deformation is controlled by an exponential degradation of the cohesion parameter fitting tensile test data which dominates the post-peak response of concrete

$$c = \frac{\sigma_t}{f_t} = \exp\left\{-5\frac{w}{w_r}\right\}. \tag{15}$$

The cohesion parameter is uncoupled in the expression of the concrete failure criterion in Equation 1 resulting in an isotropic loss of strength due to reduction of the cohesion. For $c = 1$, the material is intact and for $c = 0$, the material is considered to have lost the entire cohesive strength and thus exhibits only residual frictional shear strength in compression.

The fracture energy must remain constant and independent of the finite element size. Therefore, the mapping between the crack opening displacement w in the definition of the constant fracture energy, and the tensile cracking strain ϵ_c used at the constitutive level of the equivalent continuum leads to the definition of a length scale related to the finite element size h^e normal to the crack direction, so that $w = h^e \epsilon_c$ following the idea of the crack band model by Bažant and Oh (1983) or the composite damage model of Willam (1984). The simulation of localized failure like punching shear failure introduces this dependence on the finite element size which plays the role of a localization limiter.

Punching failure is characterized by distinct states of stress which exhibit very different ductility or rather brittleness. This difference in brittleness is included in the model by considering the number of micro-cracks formed in a specimen following the experimental observations that axial splitting in compression as well as in shear results from coalescence of many micro-cracks. The analytical formulation of the fictitious number of cracks N is derived based on the following experimental observations:

1. uniaxial tension test:
   $(\xi = f_t/\sqrt{3}, \rho = \sqrt{2/3} f_t, \theta = 0)$ is characterized by one single crack,
2. triaxial extension test:
   $(\xi = \sqrt{3} f_t, \rho = \theta = 0)$ is characterized by one single crack,
3. uniaxial compression test:
   $(\xi = -f_c/\sqrt{3}, \rho = \sqrt{2/3} f_c, \theta = \pi/3)$ is characterized by N_b cracks (introduced as a new material parameter),
4. biaxial compression test:
   $(\xi = -2f_{bc}/\sqrt{3}, \rho = \sqrt{2/3} f_{bc}, \theta = 0)$ (f_{bc} is the equi-biaxial compressive strength) is characterized by one single crack.

It should be noted that for the simulation of punching shear failure, the reproduction of the biaxial compressive state of stress is critical at the corner of the slab-column intersection. The analytical expression of the fictitious number of cracks includes the polar angle θ in order to distinguish between localized failure along the tensile meridian and distributed failure along the compressive meridian. The fictitious number of cracks is expressed in terms of the ratio ξ/ρ, so it remains constant during proportional loading. The fictitious number of cracks is written as follows for $\frac{\xi}{\rho} < 1/\sqrt{2}$:

$$N = \sqrt{2}(-\frac{\xi}{\rho} + 1/\sqrt{2})(1 - \cos\theta)(N_b - 1) + 1, \tag{16}$$

and for $\frac{\xi}{\rho} \geq 1/\sqrt{2}$ the number of cracks is $N = 1$. The four observations mentioned earlier are reproduced as illustrated in Figure 3.

The combination of radial and tangential cracks is accounted for in an average form by computing the increment of crack opening Δw as the positive norm of the plastic strain $\|\langle \Delta \epsilon_p \rangle\|$ (being the internal variable) where $\|\cdot\|$ denotes the norm and $\langle\rangle$ are the Macauley brackets which extract positive components of the argument such that $\langle \boldsymbol{x} \rangle = \sqrt{0.5(x_i + |x_i|)x_i}$. Consequently, the in-

crement of crack opening may be expressed as

$$\Delta w = h^e \Delta\gamma \| \langle \frac{\partial g}{\partial \boldsymbol{\sigma}} \rangle \| \frac{1}{N}, \qquad (17)$$

where $\Delta\gamma$ is the plastic multiplier.

Stiffness degradation due to cracking is assumed to occur only in the softening range of the response. The elastic constitutive matrix is modified in the form of equivalent degradation of Young's modulus E_o so that

$$E = c\, E_o. \qquad (18)$$

For full tensile damage ($c = 0$) reduces Young's modulus to zero. This model corresponds to a unilateral scalar damage model and is necessary to capture punching shear failure.

2.5 *Numerical implementation*

The stress integration algorithm is based on an elastic-predictor, plastic-corrector strategy. The elastic-predictor step and the plastic corrector step are evaluated with the cutting-plane algorithm developed by Ortiz and Simo (1986). A relaxation method is coupled with the cutting-plane algorithm of plastic correction in order to avoid that the stress point is returned accidentally inside the elastic domain due to exponential decohesion.

Circular reinforced concrete slabs are considered which are modeled with four node quadrilateral axisymmetric elements (quad-axi). The regularization parameter of the quad-axi (h^e) which appears in the softening formulation is the square root of the cross section area so that the circumferential direction is not taken into account. This results in a constant crack spacing along the perimeter as observed in punching failure experiments.

Mesh locking occurs as a result from near incompressibility. For the developed concrete model, the flow rule often permits only for little volume changes under high confinement, so if plastic strains become large, the response becomes nearly incompressible. This difficulty is overcome by the treatment of incompressibility developed by Hughes (1980) using the mean-dilatation formulation.

The non-linear solution is advanced in incremental load steps which require iterations. A modified Newton-Raphson algorithm is implemented with a special strategy to capture localized failure. Therefore:

- the predictor step is linear elastic in order to facilitate unloading,
- the corrector iteration is elastic for a certain number of converging iterations (norm of the out-of-balance force is reducing) and only after these elastic iterations the corrector iteration is switch to plastic,
- however, the corrector iteration is changed back to elastic as soon as divergence of the norm of the out-of-balance force is detected.

The tensile damage of the elastic concrete stiffness is assumed to remain constant during each load step. The elastic modulus is updated according to the state variables at the previously converged equilibrium configuration (not at the previous iteration). This has the advantage that no coupling between elastic degradation and plastic softening has to be considered. However, fairly small load steps are required because of the discontinuous changes of the elastic stiffness properties.

3 PUNCHING FAILURE MECHANISMS

3.1 *Description of the test problem*

The circular slab tested by Kinnunen and Nylander (1960) reinforced with ring reinforcement (denoted by IB15a) is used for the numerical simulation because of its axially symmetric geometry. The slab has a total diameter of 1840 mm and a thickness of 150 mm. Experimentally, the load is applied to the column (150 mm in diameter) by means of a hydraulic jack and transferred to the floor by mean of tie rods along a radius of 855 mm.

The finite element mesh used for the simulation is chosen such that the punching crack is eventually aligned with the mesh, but without predefining its orientation. The mesh is refined around the corner of the slab-column intersection. The load is applied by controlling the vertical displacement to capture an eventual softening.

The concrete is characterized by a mean compressive cylinder strength of f_c=28 MPa. The tensile strength is assumed to be f_t=3 MPa. The fracture energy—according to the CEB-FIP model code (1990)—depends on the maximum aggregate size (32 mm) and on the tensile strength so that G_f=120 N·m/m^2. The following parameters are assumed: Young's modulus E_0=25000 MPa, Poisson's ratio of ν=0.2, number of cracks in compression N_b=10, and dilatancy angle at the ultimate uniaxial compressive strength $\psi_c = 10^0$. The reinforcement is made of steel ribbed bars of 12 mm in diameter which are characterized by Young's modulus of 210000 MPa and a uniaxial yield strength of 450 MPa. The hardening modulus is assumed to be 10000 MPa. The positions of the ring elements are located at the nodes of the concrete finite element mesh.

The predicted punching load agrees with the experimental failure load, however the numerical model predicts a stiffer response than the one monitored experimentally. This is due to pauses dur-

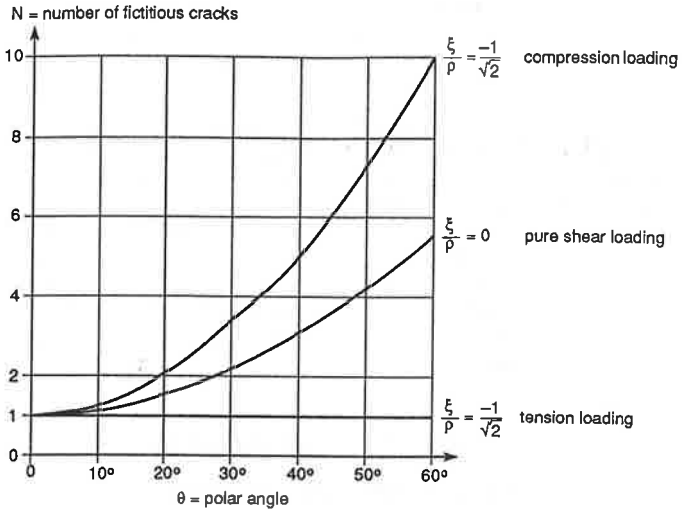

Figure 3: Variation of the fictitious number of cracks with stress invariants

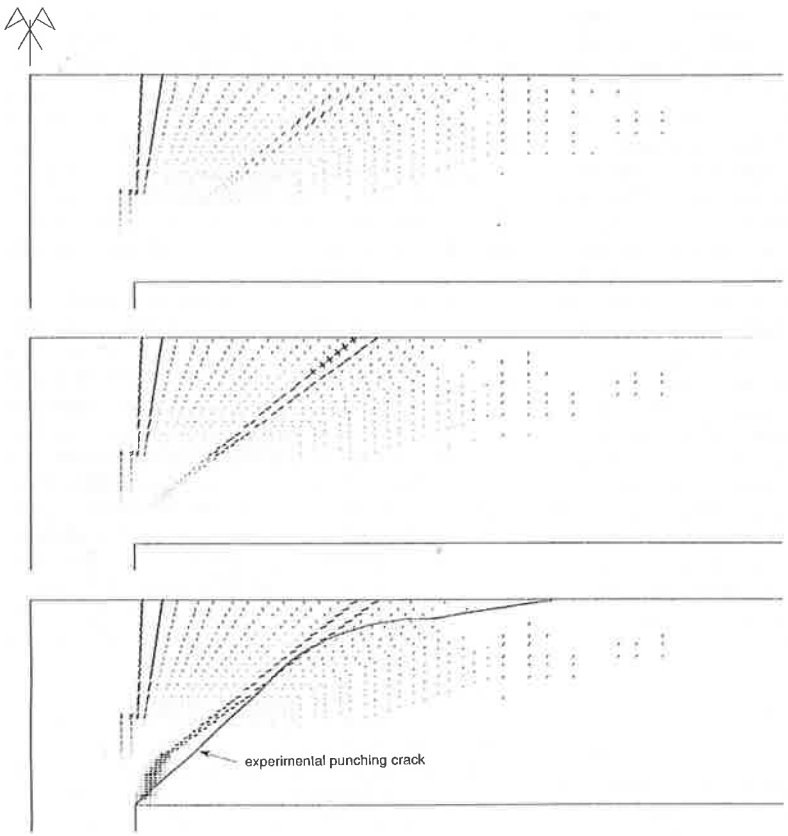

Figure 4: Progression of tangential cracks at the three last load steps

ing the load-controlled test without a closed-loop feed-back systems resulting in horizontal branches of the response curve.

3.2 *Cracking phenomenon*

The punching failure simulation reproduces the tangential cracking phenomenon presented in Figure 4 for the last three load steps. In this Figure, the tangential cracks are plotted if the principal strain is larger than the rupture deformation in uniaxial traction: f_t/E_0. The tangential cracks are symbolized at the Gauss point by straight lines for which the length is computed based on the cohesion parameter c and the size h^e of the finite element such that:

$$\text{crack length} = 0.33h^e(1-c). \tag{19}$$

The crack orientation is perpendicular to the major principal strain orientation. A stress-free crack is symbolized by a thicker line and is shown if $c < 0.007$ (corresponding to $w > w_r$).

Figure 4 shows the response for a vertical displacement of 3.1 mm corresponding to a stress-free tangential flexural crack which has opened through half the slab thickness. At that load, the first inclined stress-free crack appears inside the slab thickness, just below the reinforcement. This shows that the punching crack is initiated by micro-cracks coalescence at the top of the slab. This coalescence has been observed experimentally in the punching-shear tests of Regan (1983) who reported that micro-cracks are formed across the slab thickness before failure occurs. Along the same line, Moe (1961) observed visually the formation of inclined cracks across the slab thickness before failure occurs. By increasing the vertical displacement this inclined crack expands toward the corner of the slab-column intersection. Most of the others inclined micro-cracks close at the same timeg. At failure, the punching crack has reached the corner of the slab-column intersection.

Consequently, punching failure is initiated by micro-crack coalescence and followed by a tensile crack propagation. The ACI Committee 446 (1992) suggests that punching failure results only from a single crack propagation; however, the proposed direction of propagation is contrary to the one observed here as the punching crack is initiated at the top surface of the slab and propagates from the upper part of the slab to the bottom surface.

Finally, it may be observed that the punching crack orientation is very close to the experimental one except at the top of the slab.

3.3 *Sensitivity analysis*

First, the influence of the concrete's uniaxial tensile strength was investigated by simulating slabs with different tensile strengths (f_t=2.1, 3, and 3.9 MPa). The crack mechanisms are the same but the response curves are distinct. The behavior of the slab is stiffer for a high value of tensile strength. The load at which the first stress-free tangential flexural crack initiates increases with increasing tensile strength. Once the tangential flexural crack has formed, the slope of the load-deflection response is similar for all slabs. The failure load at which failure occurs increases with raising tensile strength.

The uniaxial concrete compressive strength does not influence the punching failure. Neither the cracking mechanism nor the response curve are modified for slabs with different uniaxial compressive strengths: f_c=22.5, 28.1, and 33.7 MPa (while the tensile strength is held constant). It can be concluded that the punching failure is due to tensile failure of concrete along the inclined punching crack, and it is not due to compressive failure of concrete. The influence of the tensile strength was already suggested by Moe (1961) who mentioned that the punching failure is very often of a splitting type, and it is comparable to the type of failure observed in specimens subjected to tension. Although the tensile and compressive strengths are known to be interrelated, the parametric study considered them to be independent of each other.

The influence of concrete fracture energy was investigated showing that it does not influence the stiffness but it influences the ductility as the maximum displacement increases with increasing fracture energy. The number of cracks in uniaxial compression, the out-of-roundness parameter and the dilatancy angle at the uniaxial ultimate compressive strength have little influence on the cracking mechanism and the response curve.

3.4 *Size-effect in punching-shear*

The size-effect was investigated by simulating four slabs of different sizes but with a similar scaling factor which applies to the concrete geometry and the steel area. Except for these dimensions, the slabs have the same boundary conditions and material characteristics. The finite element mesh is refined for large structures to avoid unstable response as the softening slope is controlled by the finite element size.

The nominal shear stress is computed as

$$\tau_n = \frac{P_{failure}}{\pi(2r_s + d)d}, \tag{20}$$

where the radius of the column is denoted by r_s and d is the slab effective depth. It is observed that the nominal shear stress decreases with increasing slab thickness illustrating size-effect.

Assuming constant fracture energy, Bažant (1984) derived a size-effect law which was shown to describe the size-effect in punching failure by Bažant and Cao (1987). This law is adjusted here to fit the four slab simulations (without having the experimental scatter) by linear regression which gives

$$\tau_n = 1.55 f_t (1 + d/34)^{-1/2}, \tag{21}$$

where f_t is the uniaxial tensile strength of concrete. This size-effect law for punching shear is characterized by two asymptotes: a horizontal branch (strength criterion) and an inclined branch (linear elastic fracture mechanic), whereby standard slabs fall into the transition region, where size-effects might become important.

3.5 *Localization analysis*

The formation of weak discontinuities (weak discontinuities indicate the formation of jumps in the strain fields, whereas strong discontinuities result in jumps not only in the strain but also in the displacement field as distinguished by Willam et al. (1994)) such as cracking in concrete can be monitored with the localization condition described by Rice (1976), Ortiz et al. (1987) and Rudnicki and Rice (1975). This localization condition in elastic-plastic material across a shear band normal to the direction $\boldsymbol{N}$ is characterized by the acoustic tensor

$$\boldsymbol{Q}_{ep} = \boldsymbol{N} \boldsymbol{D}_{ep} \boldsymbol{N}, \tag{22}$$

which is obtained by contracting the tangential material law $\boldsymbol{D}_{ep}$ with the critical normal direction $\boldsymbol{N}$ of the discontinuity. The damaged elastic-plastic constitutive matrix is an extension of the elastic-plastic tangent operator:

$$\boldsymbol{D}_{ep} = \boldsymbol{D}^n - \frac{(\boldsymbol{D}^n \boldsymbol{m})(\boldsymbol{D}^n \boldsymbol{n})^T}{-\frac{\partial f}{\partial \boldsymbol{q}} \boldsymbol{h} + \boldsymbol{n}^T \boldsymbol{D}^n \boldsymbol{m}}, \tag{23}$$

where $\boldsymbol{D}^n$ denotes the damaged elastic constitutive matrix at load step n. The damaged elastic degradation is evaluated at the previous converged load step and not at the previous iteration is considered. This results in a damaged elastic constitutive matrix which is constant during each load step. This has the advantage that no coupling between elastic degradation and plastic softening has to be considered for the computation of the damaged elastic-plastic constitutive matrix.

For localization to occur along a discontinuity normal to the direction $\boldsymbol{N}$, the acoustic tensor $\boldsymbol{Q}_{ep}$ must be singular. It has to have at least one zero eigenvalue which corresponds to the localization condition

$$\det(\boldsymbol{Q}_{ep}) = 0. \tag{24}$$

This condition also signals loss of ellipticity because it corresponds to the change of the static equilibrium equations from elliptic to hyperbolic partial differential equations. For the 2-D case, the normal to a discontinuity is defined as:

$$\boldsymbol{N} = \begin{pmatrix} \cos\alpha \\ \sin\alpha \\ 0 \end{pmatrix}. \tag{25}$$

Following the work presented by Ortiz et al. (1987) the determinant of the acoustic matrix expands for non-symmetric elastic-plastic material behavior to:

$$\begin{aligned} \det(\boldsymbol{Q}_{ep}) \;=\; & a_0 \sin^4\alpha + a_1 \sin^3\alpha\cos\alpha + \\ & a_2 \sin^2\alpha\cos^2\alpha + a_3 \sin\alpha\cos^3\alpha + \\ & a_4 \cos^4\alpha, \end{aligned} \tag{26}$$

where:

$$\begin{aligned} a_0 &= D^{ep}_{33} D^{ep}_{22} - D^{ep}_{32} D^{ep}_{23} \\ a_1 &= D^{ep}_{13} D^{ep}_{22} + D^{ep}_{31} D^{ep}_{22} - D^{ep}_{12} D^{ep}_{23} - D^{ep}_{32} D^{ep}_{21} \\ a_2 &= D^{ep}_{11} D^{ep}_{22} + D^{ep}_{13} D^{ep}_{32} + D^{ep}_{31} D^{ep}_{23} - D^{ep}_{12} D^{ep}_{21} \\ &\quad - D^{ep}_{12} D^{ep}_{33} - D^{ep}_{33} D^{ep}_{21} \\ a_3 &= D^{ep}_{11} D^{ep}_{23} + D^{ep}_{11} D^{ep}_{32} - D^{ep}_{13} D^{ep}_{21} - D^{ep}_{12} D^{ep}_{31} \\ a_4 &= D^{ep}_{11} D^{ep}_{33} - D^{ep}_{13} D^{ep}_{31}. \end{aligned}$$

and D^{ep}_{ij} are the component of the elastic-plastic constitutive matrix. The determinant of the acoustic tensor is an explicit function of the angle α. The critical orientation for which the determinant of the acoustic tensor is minimal is determined numerically. For graphical representation, the value of the determinant of the acoustic tensor is normalized by the determinant of the acoustic tensor of isotropic elasticity:

$$\det \boldsymbol{Q} = \mu(\lambda + 2\mu). \tag{27}$$

In this case, the determinant of the elastic acoustic tensor is independent of the orientation of the discontinuity.

The acoustic tensor is analyzed at the corner of the slab-column. In Figure 5, the normalized ratio of the determinant of the acoustic tensor is plotted versus the angle α for two load steps: before failure and at failure.

It is observed that before failure, the determinant of the acoustic tensor exhibits two minimum values for the inclinations: α=80^0 and 152^0. This distribution is comparable to the one reported by Willam et al. (1997) for the simple shear test, which corresponds to formation of two slip planes due to loss of frictional resistance. However, following a non-proportional loading due to internal cracking and stresses distribution, the distribution

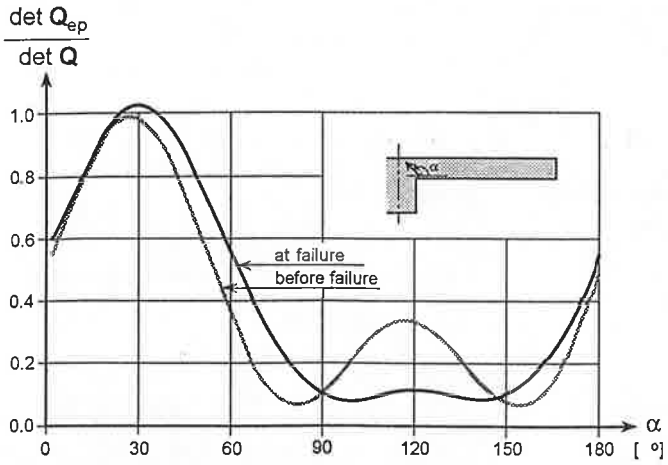

Figure 5: Evolution of the acoustic tensor at the slab-column corner for a circular slab with ring reinforcement

of the acoustic tensor at failure is characterized by a region $90^0 \leq \alpha \leq 150^0$ where $\det \boldsymbol{Q}_{ep}$ is minimal. The average value of this region reads α=120^0 which matches the inclination of the punching-shear crack. At failure, the distribution of the acoustic tensor approaches the one reported by Willam et al. (1997) for pure shear (loss of cohesion). Therefore, this indicates that punching-shear failure at that particular point of the slab, reproduces a pure shear state of stress, which corresponds to the formation of a tensile crack.

4 CONCLUSION

The proposed finite element model reproduces shear failure in reinforced concrete and allows to simulate punching-shear failure in circular slabs reinforced with ring reinforcement. The comparison with experimental results reveal that the mode of failure, characterized by a localized inclined punching crack, is properly captured. A closer look at the failure mechanisms shows that:

1. the punching crack is initiated by coalescence of micro-cracks inside the slab followed by crack propagation towards the corner of the slab-column,
2. the punching failure is caused by tensile concrete cracking along the inclined punching crack and is not the result of compressive failure of concrete,
3. the analysis of the acoustic tensor reveals that the compression-shear stress at the slab-column intersection is modified during the punching failure process and approaches a state of pure shear stress responsible for tensile crack propagation.

REFERENCES

ACI Committee 446, Fracture Mechanics, (1992). *Fracture mechanics of concrete structures: Part I, State-of-Art Report.* Bažant, Z.P. editor.

Bažant, Z.P. (1984). Size effect in blunt fracture: concrete, rock, metal. *Journal of Engineering Mechanics*, 110(4):518–535.

Bažant, Z.P. & Cao, Z. (1987). Size effect in punching shear failure of slabs. *ACI Structural Journal*, 84:44–53.

Bažant, Z.P. & Oh, B.H. (1983). Crack band theory for fracture of concrete. *Matériaux et Constructions*, 16(93):155–177.

De Borst, R. & Nauta, P. (1985). Non-orthogonal cracks in a smeared finite element model. *Engineering computation*, 2:35–46.

Chen, W.F. (1982). *Plasticity in reinforced concrete.* McGraw-Hill.

Comité Euro-International du Béton. (1990). *CEB-FIP model code.* Bulletin d'information 195-196.

Dyngeland, T., Hoiseth, K. & Opheim, E. (1994). Nonlinear analyses of reinforced concrete members subjected to punching shear *Computational*

modeling of concrete structures. Pineridge Press, H. Mang N. Bićanić R. De Borst, Euro-C conference, Innsbruck, Austria, 865-873.

González-Vidosa, F., Kotsovos, M.D. & Pavlović, M.N. (1988). Symmetrical punching of reinforced concrete slabs an analytical investigation based on nonlinear finite element modeling. *ACI Structural Journal*, 85(3):241-250.

Hillerborg, A., Modeer, M. & Petersson, P.E. (1976). Analysis of crack formation and crack growth in concrete by means of fracture mechanics and finite element. *Cement and Concrete Research (US)*, 6:773–782.

Hughes, T.J.R. (1980). Generalization of selective integration procedures to anisotropic and nonlinear media. *International Journal of Numerical Methods in Engineering*, 15:1413–1418.

Kinnunen, S. & Nylander, H. (1960). Punching of concrete slabs without shear reinforcement. Transactions 158, Royal Institute of Technology, Stockholm, Sweden.

Menétrey, Ph., Walther, R., Zimmermann, Th., Willam, K.J. & Regan, P.E. (1997). Simulation of punching failure in reinforced concrete structures. *Journal of Structural Engineering*, 123(5):652-659.

Menétrey, Ph. & Willam, K.J. (1995). A triaxial failure criterion for concrete and its generalization. *ACI Structural Journal*, 92(3):311–318.

Moe, J. (1961). Shearing strength of reinforced concrete slabs and footings under concentrated loads. Bulletin D47, Portland Cement Association.

Ortiz, M., Leroy, Y. & Needleman, A. (1987). A finite element method for localized failure analysis. *Computer Methods in Applied Mechanics and Engineering*, 61:189–214, 1987.

Ortiz, M. & Simo, J.C. (1986). An analysis of a new class of integration algorithms for elastoplastic constitutive relations. *International Journal of Numerical Methods in Engineering*, 23:353–366.

Regan, P.E. (1983). Punching shear in prestressed concrete slab bridges. Technical report, Engineering Structures Research Group, Polytechnic of Central London, England.

Regan, P.E. & Braestrup, M.W. (1985). *Punching shear in reinforced concrete.* Comité Euro-International du Béton. Bulletin d'information 168.

Rice, J.R. (1976). The localization of plastic deformation. *Theoretical and applied mechanics*, pages 207–220.

Rudnicki, J.W. & Rice, J.R. (1975). Conditions for the localization of deformation in pressure-sensitive dilatant materials. *J. Mech. Phys. Solids*, 23:371–394.

Willam, K.J. (1984). Experimental and computational aspects of concrete fracture. In *Intl. Conf. On Computed-Aided Analysis and Design of Concrete Structures*, Split.

Willam, K.J., Kang, H., Shing, B. & Spacone, E. (1997). Analysis of Shear Failure in Concrete Material. In *Material Instabilities in Solids*, IUTAM Symposium, Delft.

Willam, K.J., Műnz, Th., Etse, G. & Menétrey Ph. (1994). Failure conditions and localization in concrete. *Computational modeling of concrete structures*, Euro-C conference, Innsbruck, Austria, March 1994.

Willam, K.J. & Warnke, E.P. (1974). Constitutive model for triaxial behavior of concrete. In *Concrete structures subjected to triaxial stresses*, Bergamo. International Association for Bridges and Structural Engineering.

FROM THE SAME PUBLISHER:

Boer, G.den (ed.) 90 5410 945 9
Challenges for concrete in the next millenium – *Proceedings Of the XII FIP congress, Amsterdam, 23-29 May 1998*
1998, 25 cm, c.800 pp., 2 vols, Hfl.335 / $185.00 / £112
Topics: Development and applications of improved materials; Automated production and construction; Prestressed concrete structures; Computer aided engineering applications; Large scale testing; Assessment and upgrading of structures; Tunnels and underground structures; Education in concrete design and construction; Seismic resistant structures; Prefabrication; Protection against hazards and accidents; Sea structures and other structures; Life span analysis; Application of risk analysis; etc.

Grzebieta, R.H., R.Al-Mahaidi & J.L.Wilson (eds.) 90 5410 900 9
Mechanics of structures and materials – *Proceedings of the fifteenth Australasian conference, Melbourne, Victoria, Australia, 8-10 December 1997*
1997, 25 cm, 734 pp., Hfl.230 / $115.00 / £77
These proceedings include a selection of a broad range of research topics currently being investigated in the fields of structures, foundations and materials in Australasia. Papers cover diverse topics such as: Fibre reinforced composites; Concrete and steel composite structures; Concrete design; Steel design and welding; Dynamic, fire and seismic loading; Finite element analysis and optimisation; Stability in structures; Reliability; Timber and masonry structures; and Geomechanics.

Rots, J.G. (ed.) 90 5410 680 8
Structural masonry – *An experimental/numerical basis for practical design rules* (CUR Report 171)
1997, 25 cm, 166 pp., Hfl.175 / $95.00 / £58
The main objective was to create a basis for a general approach towards structural masonry. This objective has been met via an integration of experimental and computational techniques. Accurate displacement-controlled materials experiments have produced an extensive database of strength, stiffness and softening properties for tension, compression and shear. This data has been transferred into numerical models for simulating the deformational behaviour and failure behaviour of masonry structures. The models have been implemented into finite and distinct element codes and have been subsequently verified against shear wall experiments and analytical solutions for masonry parts.

Meskouris, K. & U.Wittek (eds.) 90 5410 927 0
Aspects in modern computational structural analysis – *Festschrift for Professor Krätzig*
1997, 25 cm, 510 pp., Hfl.195 / $99.00 / £65
A selective overview of the current state of the art in some important areas of Modern computation structural analysis and is dedicated to Prof. W.B.Krätzig on the occasion of his 65th birthday. It contains over 30 original contributions of international experts in the field, grouped under the headings of Structural dynamics; Plates, shells steel and reinforced concrete structures and General computational mechanics and computer applications. It includes papers on wind-excited structures, reduction techniques and methods for the assessment of uncertainty effects and also on numerical simulations for blast and impact protective design, three dimensional shell formulations, large inlastic strain analyses, stability and imperfection sensitivity issues, influence of steel connections and numerical analyses of reinforced and prestressed concrete structures. The largest part of the volume features papers on trends in computer-aided structural design, computational stochastic mechanics and engineering optimization, the computer simulation of blasting smokestacks, applications of artificial neural networks in structural engineering; etc.

Spanos, P.D. (ed.) 90 5410 527 5
Computational stochastic mechanics – *Proceedings of the second international conference, Athens, Greece, 12-15 June 1994*
1995, 25 cm, 784 pp., Hfl.260 / $130.00 / £87
Random processes and fields; Random vibrations (I and II); Control and optimization; Earthquake engineering; Monte Carlo methods; Stochastic finite elements; Stochastic boundary elements and continua; Applied random vibrations; Safety and reliability; Damage and fatigue; and Concrete and geotechnical applications. Editor: Rice University, Houston, TX, USA.

Shiraishi, N., M.Shinozuka & Y.K.Wen (eds) 90 5410 978 5
Structural safety and reiliability – *Proceedings of the 7th international conference, ICOSSAR'97, Kyoto, 24-28 November 1997*
1998, 25 cm, c.3000 pp., 3 vols, Hfl.395 / $195.00 / £132
Topics covered: Basic theory & methods; Design concepts; Design methods; Damage/maintenance; Earthquake; Geotechnical engineering; Materials; Social systems / Social science; Stochastic process; Structures; Wind; etc.

Stewart, M.G. & R.E.Melchers (eds) 90 5410 958 0
Integrated risk assessment: Applications and regulations – *Proceedings of the international conference, Newcastle, Australia, 7-8 May 1998*
1998, 25 cm, 154 pp., Hfl.155 / $75.00 / £52
The book describes methods for integrated risk assessments, and important and novel applications. Regulatory aspects provide a central theme to the book, particularly the way these are likely to develop in the forseeable future. Engineers, scientists, regulatory authorities and other practioners will gain valuable insights in trends in regulatory requirements, practical implementation of AS/NZS 4360-1995,, quantitative/probabilistic risk assessments and environmental risk assessments. These topics are related to the design, construction and operation of chemical and process plants, petrochemical facilities, nuclear facilities and other potentially hazardous installations.

Lydersen, S., G.K.Hansen & H.Sandtorv (eds) 90 5410 966 1
European safety and reliability – *Proceedings of the ERSEL '98 conference, Trondheim, Norway, 17-19 June 1998*
1998, 25 cm, c.1800 pp., 2 vols, Hfl.275 / $140.00 / £92
Topics covered: Ageing of components; Bayesian methods; Computer programs for risk and reliability analysis; Data collection, analysis and databases; Dependent failures; Environmental risks; Emergency planning / disaster preparedness; Safety, health and environment; Human factors and human reliability; Industrial safety; Knowledge based systems/expert judgement; Life cycle assessment, including cost/benefit analysis; Legislation, regulations, standards; PSA/QRA; Reliability methods in design, operation and maintenance; RAM assessments; Risk analysis methods; Risk perception and communication; Safety management; Software reliability; Structural reliability; Systems safety, reliability and maintainability; Uncertainty and sensitivity analysis; Vulnerability analysis; etc.

Katz, Casimir & Byron Protopsaltis (eds.) 90 5410 954 8
Software für Statik und Konstruktion, Band II – *Berichte des 9.SOFiSTiK Anwender Seminars, Nürnberg, Juni 1997*
1998, 25 cm, c.400 pp., Hfl.165 / $85.00 / £55
Dieses Buch zeigt die praktischen Einsatzmöglichkeiten der Finite Elemente Methode anhand des europaweit kommerziell verfügbaren Programmsystems SOFiSTiK mit seinem breiten Anwendungsspektrum. Die Beiträge kommen aus den Bereichen: Anwendungen der Finite Elemente Methode in der Baupraxis; Tunnelbau; Brückenbau; Stahlbau; Hochbau; Leichte- und Membrantragwerke; CAD und Datenaustausch in der Tragwerksplanung.

All books available from your bookseller or directly from the publisher:
A.A. Balkema Publishers, P.O. Box 1675, NL-3000 BR Rotterdam, Netherlands (Fax: +31-10-413-5947)
For USA & Canada: A.A. Balkema Publishers, Old Post Rd, Brookfield, VT 05036-9704 (Fax: 802-276-3837)